Zero Electron Kinetic Energy Spectroscopy and Theoretical Calculations of $InNH_3$

Gretchen K. Rothschopf, Jimmye Shannon Perkins, Shenggang Li, and Dong-Sheng Yang*

Department of Chemistry, University of Kentucky, Lexington, Kentucky 40506-0055

Received: May 24, 2000; In Final Form: July 5, 2000

$InNH_3$ has been studied with single-photon zero electron kinetic energy (ZEKE) spectroscopy and density functional theory and ab initio calculations. The ZEKE spectrum reveals vibrational structures of the cation and neutral complexes. The comparison of the experiment and theory establishes that the indium-ammonia complex is a simple adduct. The adduct has a C_{3v} $^1A_1$ ground state in the ion and a C_s $^2A'$ ground state in the neutral. The lower symmetry of the neutral molecule arises from a Jahn−Teller distortion. The ionization energy of the $^2A'$ state is 39 689(3) cm^{-1}. The indium−ammonia stretch frequency is 234 cm^{-1} in the $^1A_1$ state and 141 cm^{-1} in the $^2A'$ state. The stronger metal−ligand bonding in the ion state is attributed to the additional charge−dipole and covalent interactions.

I. Introduction

Group III nitrides form the material systems for solid-state optoelectronic devices and are used extensively in high-speed, high-frequency applications.[1,2] Chemical vapor deposition with ammonia is an important process to grow metal nitride materials.[3] In this process, the formation of metal species with ammonia and the cracking of ammonia in the gas phase influence the growth rates and properties of metal nitrides.[4,5] There has been considerable interest in the reactions of group III metal atoms with ammonia and in the species formed in such reactions. Studies have been reported on the reaction of laser-ablated aluminum atoms with ammonia as characterized with electron paramagnetic resonance (ESR)[6] and FTIR[7] in argon matrices and with single-photon photoionization efficiency (PIE)[8] and resonant two-photon ionization (R2PI)[9] in the gas phase. Although the ESR and FTIR experiments detected inserted or dehydrogenated products in argon matrices, the PIE and R2PI measurements showed the formation of association complexes in the gas phase. Several ab initio calculations have also been reported on the ground-state geometries and energetics of aluminum-ammonia compounds.[10−13] Both association and insertion complexes have been predicted to be stable although the inserted structure $HAlNH_2$ is lower in energy. The association complex $AlNH_3$ has been calculated to be Jahn−Teller distorted from C_{3v} symmetry in its ground state. The energy barrier to form the insertion product $HAlNH_2$ has been estimated to be in the range of 23−34 kcal/mol.

In contrast, there has been only one report on the reaction of the In atom with NH_3 as studied with PIE spectroscopy.[14] In that study, the authors estimated the ionization potential (IP) of $InNH_3$ and the frequency difference of the metal−ligand stretches in the ion and neutral. However, because of the limited spectral resolution, fine vibrational structure and precise energy are usually not obtainable from such PIE measurements. Recently, we reported the zero electron kinetic energy (ZEKE) spectrum of $AlNH_3$ formed by the reaction of laser-ablated aluminum atoms and ammonia in gaseous molecular beams.[15] From the spectrum, we obtained the precise IP, spin−orbit splitting, and Al−NH_3 stretch frequency of the neutral and the metal−ligand stretch and bend frequencies of the cation. This article presents the first ZEKE study of $InNH_3$ in combination with quantum chemical calculations.

II. Experimental and Computational Methods

A. Experimental Details. Figure 1 presents the schematic of the metal cluster beam ZEKE apparatus. It consists of two vacuum chambers. The first chamber houses a Smalley-type cluster source[16] pumped by a 2200 L/s oil diffusion pump (Edwards). The second chamber houses the ZEKE spectrometer pumped by two 400 L/s turbomolecular pumps (Seiko Seiki). A gate valve separates the two chambers. The cluster source consists of a piezoelectric pulsed valve to deliver intense gas pulses,[17] a motor driven mechanism to rotate and translate a metal rod to ensure each laser pulse vaporizes a fresh surface of the metal target, a clustering tube to help maximize the production of the species of interest, a homemade skimmer to collimate the molecular beam, and a pair of charged deflection plates to remove residual ionic species from the molecular beam before it enters the second chamber. The ZEKE spectrometer is a two-field, space-focused, Wiley−McLaren time-of-flight mass spectrometer.[18] It consists of a two-stage extraction assembly, a 34 cm long flight tube, and a dual microchannel plate detector (Galileo). The entire spectrometer is housed in a cylindrical, double-walled, μ-metal shield to isolate it from the earth's magnetic field.

Indium−ammonia complexes were produced with a Nd:YAG laser (532 nm, Quanta-Ray GCR-3) vaporization of an indium rod (99.999%, Aldrich) in the presence of a pulse of helium gas doped with ~2% of ammonia (99.99%, Matheson). The resulting molecules in the molecular beam were identified with single-photon photoionization time-of-flight mass detection. The production of the 1:1 $InNH_3$ complex was maximized by optimizing the time and power of the vaporization and ionization lasers, the reactant concentration, and the backing pressure of the carrier gas. The ionization threshold of $InNH_3$ was located by recording the ion signal as the frequency-doubled dye laser (Lumonics HD-500) was scanned in the 37 700−40 700 cm^{-1} range.

ZEKE measurements were carried out by first photoexcitation of the molecule to high-lying Rydberg levels and then pulsed-

* To whom correspondence should be addressed. E-mail: dyang0@pop.uky.edu. Fax: (859) 323-1069.

10.1021/jp001916v CCC: $19.00
Published on Web 08/08/2000

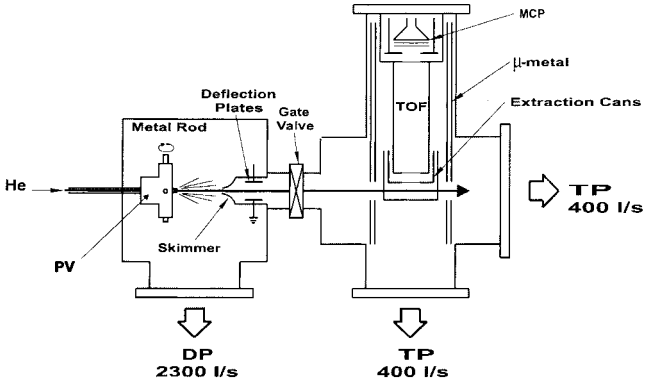

Figure 1. Schematic of the metal cluster ZEKE spectrometer system. PV, pulsed valve; DP, diffusion pump; TP, turbomolecular pump; TOF, time-of-flight tube; MCP, microchannel plate.

field-ionization of the Rydberg states. A typical field of 1.2 V/cm was applied 3 μs after the laser excitation for 100 ns. The resulting ZEKE electron signal was capacitively decoupled from the dual microchannel plate anode, amplified by a preamplifier (Stanford SR445), averaged to 30 shots per data point by a gated integrator (Stanford SR250), and collected in a computer. The ZEKE spectra were recorded as a function of the laser wavelength. The laser wavelengths were calibrated against vanadium atomic transitions. We also measured the ZEKE transitions with the electric fields in the 0.6−1.2 V/cm range and observed little change in the peak position.

B. Computational Method. Gaussian 98 program package[19] was used in our quantum chemical calculations to compare with the spectroscopic measurements. Geometries and harmonic vibrational frequencies were calculated with three methods: Becke's three parameter hybrid functional with the gradient corrections of Perdew (B3P86), Becke's three parameter hybrid functional with the correlation functional of Lee, Yang, and Parr (B3LYP), and quadratic configuration interaction including all single and double excitations (QCISD). These calculations were carried out with the LanL2DZ basis for the indium atom and the 6-311+G(d,p) basis for the nitrogen and hydrogen atoms.

Multidimensional Franck−Condon (FC) factors were calculated from the equilibrium geometries, harmonic frequencies, and normal modes determined by the quantum chemical calculations for the neutral and monopositive ion. In these calculations, the Duschinsky[20] effect was considered to account for the normal mode differences in the neutral and ion molecules. Details of the FC calculations were previously described.[21] Spectral broadening was simulated by giving each line a Lorenztian line shape with a full width at half-maximum (fwhm) of 6.0 cm^{-1}, the line width of the experimental spectra. Boltzmann factors were used to simulate finite temperature spectra.

III. Results and Discussion

A. Spectroscopic Measurements. Figure 2 presents the single-photon PIE spectrum of $InNH_3$. The ion signal was recorded as a function of laser wavelength. The general features of the spectrum are similar to those reported previously.[14] The IP of the complex is estimated to be 39 670(50) cm^{-1}, as indicated by the arrow. This value is corrected by +110 cm^{-1} for the shift induced by the dc extraction field of 320 V/cm in the extraction region. Above the onset, the spectrum displays some structural features, which may be attributed to the vibronic transitions but are difficult to assign.

Figure 3a shows the single-photon ZEKE spectrum (fwhm = 6.0 cm^{-1}) of $InNH_3$ in the range of 39 400−40 600 cm^{-1}.

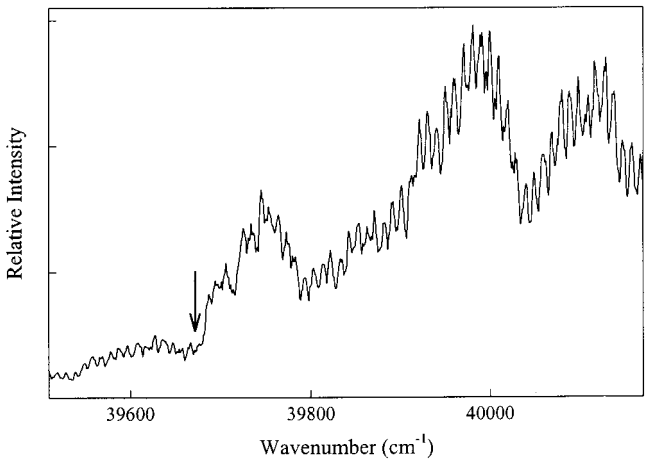

Figure 2. The photoionization efficiency spectrum of $InNH_3$. The ionization threshold is shown by the arrow. The wavenumbers are corrected by the shift induced by the ionization field, see text.

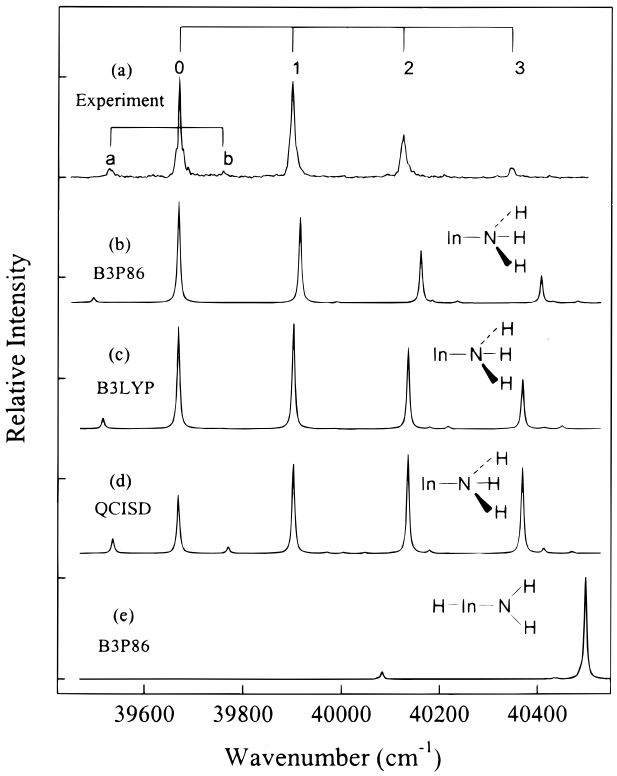

Figure 3. Experimental (a) and simulated (b−e) spectra of indium-ammonia complexes. The simulations (b−d) were obtained from the association structures calculated by the B3P86, B3LYP, and QCISD methods, whereas the simulation (e) was calculated from the inserted structure of the B3P86 calculations. All simulations were carried out with the temperature of 100 K.

Beyond this energy region, no wavelength-dependent signal was detected. The spectrum consists of a main progression (*bands labeled 0−3*) with the lowest energy band at 39 689(3) cm^{-1} and energy intervals of about 230 cm^{-1}. In addition, the spectrum shows a weak band, a, located at 141 cm^{-1} to the red of the first strong band. At 230 cm^{-1} above the band a, a smaller feature, b, may also be identified. Table 1 lists the energy positions of the ZEKE bands without electric field corrections.

The ZEKE bands can be discussed in terms of the vibronic transitions from the neutral to the ion complex. The 230 cm^{-1} vibrational interval is well below the known vibrational frequencies of ammonia and must be associated with a metal−ligand

TABLE 1: Band Positions (cm^{-1}) Obtained from the ZEKE Spectrum of $InNH_3$

position	$\nu_s^+ - \nu_s$[a]
39 548.1	0−1
39 689.0	0−0
39 777.8	1−1
39 918.6	1−0
40 144.8	2−0
40 366.0	3−0

[a] ν_s^+ and ν_s are the vibrational quanta of the In^+-NH_3 and $In-NH_3$ stretch modes.

vibration. Because the molecular beam is cold, the neutral complex is not expected to be highly populated thermally. Therefore, the main progression (*bands 0−3*) is associated with the vibrational coordinates in the ion state, whereas the 141 cm^{-1} interval is related to the vibrational coordinates in the neutral complex. The energy position, 39 689(3) cm^{-1}, of the band *0* corresponds to the IP of the neutral complex, which agrees with the values obtained from the current and previous PIE measurements, of course, with a much higher precision. If the molecule probed in the ZEKE experiments is an association complex, the ZEKE spectrum of $InNH_3$ may be assigned in comparison with the spectrum of $AlNH_3$.[15] The 230 and 141 cm^{-1} intervals can be attributed to the $In-NH_3$ stretch in the ion and neutral species, respectively. By fitting the ZEKE band positions to $G(v) = \omega_s^+(v^+ + 1/2) - \omega_s^+x_s^+(v^+ + 1/2)^2$, the harmonic frequency and anharmonicity of the ion stretch mode are obtained to be 234.1(7) and 2.1(2) cm^{-1}. However, on the basis of this preliminary assignment, the ion stretch frequency is considerably lower than the value, 310 cm^{-1}, predicted by a previous calculation.[14] Also, the difference in the ion and neutral stretch frequencies, 93 cm^{-1}, is much smaller than the value, 150 cm^{-1}, suggested by a previous PIE study.[14] To address these discrepancies and extract more details from the spectroscopic measurements, we have carried out theoretical vibrational analysis. The results are presented below.

B. Theoretical Geometries and Vibrational Frequencies. *$InNH_3^+$ and $InNH_3$.* The minimum energy geometries, harmonic frequencies, dissociation energies, and IP values are calculated with the B3LYP, B3P86, and QCISD methods and the LanL2DZ basis for the In atom and the 6-311G+(d,p) basis for the N and H atoms. All three methods predict $InNH_3^+$ to be C_{3v} symmetry with a $^1A_1$ ground state. The $^1A_1$ state arises from the interaction of the In^+ ^1S ($5s^2$) and NH_3 $^1A_1$ ground states. Adding an electron to $InNH_3^+$ leads to doublet electronic states. Assuming that $InNH_3$ also has C_{3v} symmetry, two electronic states $^2A_1$ and ^2E can be derived from the interactions of the In ^2P ($5p^1$) and NH_3 $^1A_1$ ground states. In a coordinate system where the *z*-axis is placed along the C_3 symmetry axis, both the In p_z electron and the nitrogen lone-pair are on the molecular axis in the $^2A_1$ state, whereas the In p_x or p_y electron is off-axis in the ^2E state. Because the stronger repulsion between the p_z electron and the lone-pair, the $^2A_1$ state is expected to be less stable, and the ^2E state is expected to be the ground state. However, an orbitally degenerate state is electronically unstable and tends to undergo Jahn−Teller distortion, resulting in a lower geometric symmetry and the removal of the orbital degeneracy. Our calculations indeed predict that the H−N−H angle in $InNH_3$ is distorted from C_{3v} symmetry by up to 2.0° (Table 2), resulting in a C_s $^2A'$ ground state for the neutral complex. The Jahn−Teller distortion of the neutral complex is also evident from the e symmetry of the lowest unoccupied orbital in $InNH_3^+$. A similar Jahn−Teller distortion has also been suggested previously in $AlNH_3$.[10,11] Table 2 lists the geometries, harmonic frequencies, and dissociation energies of the $^2A'$ state of $InNH_3$ and the $^1A_1$ state of $InNH_3^+$, as well as the IP of the neutral complex.

$HInNH_2^+$ and $HInNH_2$. The inserted ion complex $HInNH_2^+$ has a $^1A_1$ ground state in C_{2v} symmetry, whereas the neutral $HInNH_2$ has a $^2A'$ ground state in C_s symmetry. Depending on the calculation methods, the $^1A_1$ state of $HInNH_2^+$ is predicted to be in the range 55−64 kcal/mol above the $^1A_1$ ground state of $InNH_3^+$, and the $^2A'$ state of $HInNH_2$ is 9−11 kcal/mol higher than the $^2A'$ state of $InNH_3$. The relative energy order of the inserted $HInNH_2$ and associated $InNH_3$ complexes is reversed from that of the corresponding aluminum complexes, for which $HAlNH_2$ was calculated to be more stable than $AlNH_3$ by 20.5 kcal/mol (B3LYP)[22] or 23.1 kcal/mol (CISD).[11] The energy barrier to form $HInNH_2$ is estimated to be 33 kcal/mol with the B3LYP calculation. Furthermore, $HInNH_2$ has a higher IP and larger In−N stretch frequency than $InNH_3$. Table 3 lists the geometries, vibrational frequencies, and IP of the insertion isomer.

C. ZEKE Spectral Assignment and Discussion. *ZEKE Spectral Assignment.* The preliminary spectral assignments presented in section IIIA are now discussed in comparison with the theoretical results. We shall first identify the carrier of the ZEKE spectrum by comparing the experimental and theoretical vibrational frequencies, FC intensity profiles, and IPs. The theoretical metal−ligand stretch frequencies of $InNH_3^+$ and $InNH_3$ are in good agreements with the experimental frequencies of 234 and 141 cm^{-1}, whereas $HInNH_2^+$ and $HInNH_2$ have no symmetric modes near the observed frequencies. Figure 3 compares the experimental spectrum and theoretical simulations, which are calculated with the geometries, harmonic frequencies, and normal modes from the B3P86, B3LYP, and QCISD methods. The comparison of the theoretical and experimental FC structures, although not perfect, clearly shows that the carrier of the ZEKE spectrum is the association complex $InNH_3$, rather than the insertion product $HInNH_2$. Furthermore, the calculated IP (4.83 eV) of $InNH_3$ with B3LYP has a good agreement with the experimental value (4.921 eV). Therefore, the assignment presented in section IIIA is confirmed: the 234 cm^{-1} progression is attributed to the In^+-NH_3 stretch, whereas the 141 cm^{-1} interval to the $In-NH_3$ stretch. The fact that the inserted complex $HInNH_2$ is not observed may suggest a high energy barrier in forming the isomer or its high ionization energy. The barrier is calculated to be >30 kcal/mol, and the IP is predicted to be >6.4 eV, which is beyond the wavelength region of our dye laser. However, because the molecular beam is cold, it is unlikely to form a significant amount of the insertion complex by considering the calculated energy barrier.

With the above spectral assignment, we can now discuss the relative accuracy of the theoretical methods used in this work. Table 4 lists the experimental and corresponding to theoretical spectroscopic constants. The three methods produce similarly overall good agreements with the experimental bond energy differences and stretch frequencies, with the B3LYP frequencies having the best match to the measured values. The bond energy difference from the experiment is calculated with the energy cycle $D_0^+(In^+-NH_3) - D_0(In-NH_3) = IP(M) - IP(InNH_3)$. The theoretical bond dissociation energies are the differences between the reactants and the association complex including the zero point vibrational energy corrections. Second, the B3LYP calculation gives the best IP, whereas the B3P86 IP is too high and the QCISD value is too low. Third, The B3P86 FC structure (Figure 3b) has the best agreement with the experimental intensity profile, while the QCISD FC progression

TABLE 2: Theoretical Equilibrium Geometries (Bond Distance, Å; Angle, Degree), Harmonic Vibrational Frequencies (cm^{-1}), Dissociation Energies (D_0, kcal/mol) of $InNH_3^+$ (C_{3v}) and $InNH_3$ (C_s) and IP (eV) of $InNH_3$

	B3LYP	B3P86	QCISD
$InNH_3^+/InNH_3$	$InNH_3^+/InNH_3$	$InNH_3^+/InNH_3$	$InNH_3^+/InNH3$
In−N	2.523/2.709	2.502/2.662	2.556/2.767
N−H	1.021/1.017 & 1.016	1.020/1.015 & 1.014	1.021/1.017 & 1.016
∠H−N−H	105.9/107.9 & 106.9	105.9/107.9 & 107.0	105.1/106.9 & 105.9
∠In−N−H	112.9/110.1 & 113.7	112.9/110.0 & 113.8	113.6/110.0 & 117.0
N−H stretch, a_1/a'	3430/3465	3453/3490	3474/3499
H−N−H bend, a_1/a'	1289/1119	1286/1118	1335/1193
In−NH_3 stretch, a_1/a'	234/153	246/171	217/132
N−H stretch, e/a′ & a″	3526/3587 & 3566	3556/3618 & 3604	3574/3626 & 3616
H−N−H bend, e/a′ & a″	1669/1665 & 1492	1665/1659 & 1530	1663/1659 & 1609
In−NH_3 bend, e/a′ & a″	511/292 & 285	516/308 & 299	497/314 & 177
D_0	29.1/6.4	31.3/8.1	24.9/6.2
IP ($InNH_3$)	4.83	5.32	4.21

TABLE 3: Theoretical Equilibrium Geometries (Bond Distance, Å; Angle, Degree) and Harmonic Vibrational Frequencies (cm^{-1}) of $HInNH_2^+$ (C_{2v}) and $HInNH_2$ (C_s) and IP (eV) of $HInNH_2$

	B3LYP	B3P86	QCISD
$HInNH_2^+/HInNH_2$	$HInNH_2^+/HInNH_2$	$HInNH_2^+/HInNH_2$	$HInNH_2^+/HInNH_2$
In−H	1.658/1.762	1.663/1.764	1.661/1.752
In−N	1.890/2.001	1.888/1.996	1.894/1.998
N−H	1.012/1.012 & 1.011	1.011/1.011 & 1.009	1.011/1.011 & 1.010
∠In−N−H	124.3/124.4 & 125.4	124.3/124.5 & 125.3	124.5/124.9 & 125.6
∠H−In−N	180.0/115.0	180. 0/115.1	180.0/114.6
∠H−N−H	111.3/110.1	111.4/110.2	111.1/109.5
N−H stretch, a_1/a'	3554/3556	3579/3688	3609/3601
In−H stretch, a_1/a'	1971/1590	1960/1599	1931/1624
H−N−H bend, a_1/a'	1561/1551	1554/1545	1578/1574
In−NH_2 stretch, a_1/a'	671/544	676/425	669/553
H−In−NH_2 out-of-plane bend, b_1/a''	479/424	475/551	451/447
H−In−NH_2 out-of-plane torsion, b_1/a''	213/265	204/261	103/278
N−H stretch, b_2/a'	3644/3656	3673/3688	3701/3698
NH_2 rock, b_2/a'	765/677	764/676	770/697
H−In−NH_2 in-plane bend, b_2/a'	416/427	415/425	398/446
IP ($HInNH_2$)	6.76	7.31	6.48

TABLE 4: Experimental and Theoretical Spectroscopic Constants of the Indium−Ammonia Complex

	experiment	B3LYP	B3P86	QCISD
IP, eV	4.9210	4.83	5.32	4.21
$\Delta(D_0^+ - D_0)$, kcal/mol	20.0	22.7	23.2	18.7
In^+-NH_3 stretch, cm^{-1}	234	234	246	217
In−NH_3 stretch, cm^{-1}	141	153	171	132

TABLE 5: IPs (cm^{-1}), Metal−Ammonia Stretch Frequency (cm^{-1}), and Estimated Force Constants (N/m) Obtained from the ZEKE Spectra of $InNH_3$ and $AlNH_3$[a]

	IP (M)[b]	IP (MNH_3)	vibrational frequency		force constant	
			M^+-NH_3	M-NH_3	M^+-NH_3	M-NH_3
$InNH_3$	46 670	39 689	234	141	48	17
$AlNH_3$[a]	48 278	39 746	339	227	71	32

[a] From ref 15. [b] From ref 25.

appears somewhat too long. Superior FC structures from B3P86 geometries have also been seen previously in the simulations of metal cluster compounds,[23,24] though it seems surprising that the simple FC model works reasonably well even for such a weakly bound molecule as $InNH_3$. The differences among the three sets of the simulations reflect the differences in the calculated geometries and show how sensitive the ZEKE spectra are to such structural differences. Nevertheless, the most prominent features of the simulated spectra from the association complex are in good agreement with each other and with experiment, providing a strong indication that the conformation probed in the experiments is indeed the adduct structure.

Electrostatic and Orbital Interactions. Table 5 lists the IP and vibrational frequencies of $InNH_3$ obtained from the ZEKE spectrum. The IP of $InNH_3$ is 0.8655 eV lower than that of the In atom. The large IP reduction upon the ligand coordination indicates the indium−ammonia bonding is much stronger in the ion than in the neutral complex. The enhanced metal−ligand binding in the ion is also evidenced from the In^+-NH_3 and In−NH_3 stretch frequencies. The bonding difference can be understood with the consideration of the additional charge−dipole attraction in the ion complex. The question, however, is whether the bonding between indium and ammonia has any contribution from orbital overlap or simply because of the electrostatic force. To address this question, we have performed a Mulliken population analysis with the B3LYP method and found only a 0.02 overlap population between In and N in the $^2A'$ neutral state, but a population of 0.40 in the $^1A_1$ ion state. The highest occupied orbital is essentially the pure In 5p character in the $^2A'$ state, whereas it is a mixture of 55% In 5s (with small $5p_z$) and 45% N lone-pair (2s2p) in the $^1A_1$ state. Thus, the population analysis indicates that the covalent interaction contributes little to the metal−ligand bonding in the neutral, but significantly in the ion complex.

The metal−ammonia bonding may be further discussed by comparing the spectroscopic constants of $InNH_3$ and $AlNH_3$.[15] The IP of $InNH_3$ is measured to be 6981 cm^{-1} lower than that of the In atom, whereas the IP of $AlNH_3$ is 8532 cm^{-1} less than that of the Al atom. To compare the strengths of the $M-NH_3$ (M = Al and In) interactions, we have converted the metal−ligand stretch frequencies to the force constants by

approximating the complexes as diatomic molecules in which NH_3 is treated as a "single atom". The approximation should be reasonable because the N−H or H−N−H vibrations within NH_3 require much higher energy than the M−N stretches, and thus, the measured frequencies should be predominantly associated with the M−N vibrations. Table 5 lists the force constants, as calculated with $k = 4\pi^2c^2\omega^2\mu$, where ω is vibrational frequencies and μ is reduced masses. These constants clearly show the In^+-NH_3 or $In-NH_3$ bonding is much weaker than the corresponding Al^+-NH_3 or $Al-NH_3$ bonding. The larger Al^+-NH_3 force is understandable because the higher charge density (or smaller atomic radius) of Al^+ than that of In^+ leads to stronger charge−dipole attraction between Al^+ and NH_3 than between In^+ and NH_3. However, the stronger $Al-NH_3$ interaction seems surprising from a purely electrostatic viewpoint because the polarizability of the aluminum atom ($\alpha_{Al} = 6.8 \times 10^{-24}$ cm^3) is smaller than that of the indium atom ($\alpha_{In} = 10.2 \times 10^{-24}$ cm^3),[25] which would have resulted in a weaker dipole/dipole-induced interaction in $Al-NH_3$ than in $In-NH_3$. As discussed above, there is basically no orbital overlap between In and N, indicating the covalent character in the In−N bonding is negligible. However, a Mulliken analysis on $AlNH_3$ has showed a 0.23 population between Al and N, making an additional covalent contribution to the Al−N bonding.[22] Therefore, the orbital overlap should be considered in discussing the bonding differences between the $InNH_3$ and $AlNH_3$ complexes.

IV. Conclusions

The single-photon ZEKE measurements, along with the theoretical calculations, identify the formation of the association complex $InNH_3$. The complex has C_{3v} symmetry with a $^1A_1$ ground state in the cation and C_s symmetry with a $^2A'$ ground state in the neutral. The IP of $InNH_3$ is 39 689(3) cm^{-1}, which is 6981 cm^{-1} lower than that of the In atom. The indium-ammonia stretch frequency is $\omega_s^+ = 234.1(7)$ cm^{-1} and $\omega_s^+x_s^+ = 2.1(2)$ cm^{-1} in $InNH_3^+$ and $\nu_s = 141$ cm^{-1} in $InNH_3$. The IP reduction upon NH_3 coordination and the stretch frequency increase upon ionization show that the indium−ammonia bonding is significantly strengthened in the ion complex. The stronger In^+-NH_3 bonding is suggested to arise from the additional charge−dipole and covalent interactions between In^+ and NH_3, which are absent in the corresponding neutral complex. A comparison of the experiment and theory indicates that with the LanL2DZ basis for the indium and the 6-311G+(d,p) basis for the nitrogen and hydrogen atoms, the B3LYP method produces a better IP of the complex than the B3P86 and QCISD methods.

Acknowledgment. Support for this work was provided by the donors of the Petroleum Research Fund, administrated by the American Chemical Society, and by the University of Kentucky Center of Computational Sciences.

References and Notes

(1) Akasaki, I.; Amano, H. *J. Electrochem. Soc.* **1994**, *141*, 2266.

(2) Mohammad, S. N.; Salvador, A. A.; Morkoc, H. *IEEE Proc.* **1995**, *83*, 1306.

(3) Hoffman, D. M. *Polyhedron* **1994**, *13*, 1169.

(4) Thon, A.; Kuech, T. F. *Appl. Phys. Lett.* **1996**, *69*, 55.

(5) Liu, S. S.; Stevenson, D. A. *J. Electrochem. Soc.* **1978**, *125*, 1161.

(6) Howard, J. A.; Joly, H. A.; Edwards, P. P.; Singer, R. J.; Logan, D. E. *J. Am. Chem. Soc.* **1992**, *114*, 474.

(7) Lanzisera, D. V.; Andrews, L. *J. Phys. Chem. A* **1997**, *101*, 5082.

(8) Di Palma, T. M.; Latini, A.; Satta, M.; Varvesi, M.; Giardini, A.*Chem. Phys. Lett.* **1998**, *284*, 184.

(9) Jakubek, J. Simard, B. *J. Chem. Phys.* **2000**, *112*,1733.

(10) Sakai, S. *J. Phys. Chem.* **1992**, *96*, 8369.

(11) Davy, R. D.; Jaffrey, K. L. *J. Phys. Chem.* **1994**, *98*, 8930.

(12) Stöckight, D. *Chem. Phys. Lett.* **1996**, *250*, 387.

(13) Fängström, T.; Lunell, S.; Kasai, P. H.; Eriksson, L. A. *J. Phys. Chem. A* **1998**, *102*,1005.

(14) Di Palma, T. M.; Latini, A.; Satta, M.; Giardini, A. *Eur. Phys. J. D* **1998**, *4*, 225.

(15) Yang, D. S.; Miyawaki, J. *Chem. Phys. Lett.* **1999**, *313*, 514.

(16) Dietz, T. G.; Duncan, M. A.; Powers, D. E.; Smalley, R. E. *J. Chem. Phys.* **1981**, *74*, 6511.

(17) Proch, D.; Trickl, T. *Rev. Sci. Instrum.* **1989**, *60*, 713.

(18) Wiley, W. C.; McLaren, I. H. *Rev. Sci. Instrum.* **1955**, *26*, 1150.

(19) Frisch, M. J.; Trucks, G. W.; Schlegel, H. B.; Scuseria, G. E.; Robb, M. A.; Cheeseman, J. R.; Zakrzewski, V. G.; Montgomery, Jr. J. A.; Stratmann, R. E.; Burant, J. C.; Dapprich, S.; Millam, J. M.; Daniels, A. D.; Kudin, K. N.; Strain, M. C.; Farkas, O.; Tomasi, J.; Barone, A.; Cossi, M.; Cammi, R.; Mennucci, B.; Pomelli, C.; Adamo, C.; Clifford, S.; Ochterski, J.; Petersson, G. A.; Ayala, P. Y.; Cui, Q.; Morokuma, K.; Malick, D. K.; Rabuck, A. D.; Raghavachari, K.; Foresman, J. B.; Cioslowski, J.; Ortiz, J. V.; Baboul, A. G.; Stefanov, B. B.; Liu, G.; Liashenko, A.; Piskorz, P.; Komaromi, I.; Gomperts, R.; Martin, R. L.; Fox, D. J.; Keith, T.; Al-Laham, M. A.; Peng, C. Y.; Nanayakkara, A.; Gonzalez, C.; Challacombe, M.; Gill, P. M. W.; Johnson, B.; Chen, W.; Wong, M. W.; Andres, J. L.; Gonzalez, C.; Head-Gordon, M.; Replogle, E. S.; Pople, J. A. *Gaussian 98*, Revision A.7; Gaussian, Inc.: Pittsburgh, PA, 1998.

(20) Duschinsky, F. *Acta Physicochim. URSS 7*, **1937**, 551.

(21) Yang, D. S.; Hackett, P. A. *J. Electron Spectrosc. Relat. Phenom.* **2000**, *106*, 153.

(22) Yang. D. S. Unpublished results.

(23) Yang, D. S.; Zgierski, M. Z.; Rayner, D. M.; Hackett, P. A.; Martinez, A.; Salahub, D. R.; Roy, P. N.; Carrington Jr., T. *J. Chem. Phys.* **1995**, *103*, 5335.

(24) Yang, D. S.; Zgierski, M. Z.; Bérces, A.; Hackett, P. A.; Roy, P. N.; Martinez, A.; Carrington Jr., T.; Salahub, D. R.; Fournier, R.; Pang, T.; Chen, C. *J. Chem. Phys.* **1996**, *105*, 10663.

(25) Lide, D. R.; Frederikse, H. P. R. *CRC Handbook of Chemistry and Physics*, 78th ed.; CRC Press: New York, 1997.